

Symmetric Improved Estimators for Continuous-time Quantum Monte Carlo

J. Kaufmann,^{1,2,*} P. Gunacker,^{1,*} A. Kowalski,³ G. Sangiovanni,⁴ and K. Held¹

¹Institute for Solid State Physics, TU Wien, 1040 Vienna, Austria

²Institute for Theoretical Solid State Physics, IFW Dresden, 01069 Dresden, Germany

³Institut für Theoretische Physik und Astrophysik,
Universität Würzburg, 97074 Würzburg, Germany

⁴Institut für Theoretische Physik und Astrophysik and Würzburg-Dresden Cluster of Excellence ct.qmat,
Universität Würzburg, 97074 Würzburg, Germany

(Dated: June 4, 2019)

We derive equations of motion for Green's functions of the multi-orbital Anderson impurity model by differentiating symmetrically with respect to all time arguments. The resulting equations relate the one- and two-particle Green's function to correlators of up to six particles at four times. As an application we consider continuous-time quantum Monte Carlo simulations in the hybridization expansion, which hitherto suffered from notoriously high noise levels at large Matsubara frequencies. Employing the derived symmetric improved estimators overcomes this problem.

PACS numbers: 71.27.+a, 02.70.Ss

I. INTRODUCTION

The Hubbard model (HM)[1] and the Anderson impurity model (AIM)[2], which are related through the dynamical mean-field theory (DMFT)[3], are two of the basic models for strongly correlated electrons. Thus, numerical and analytic solutions of these models over a wide range of parameters are of great interest in condensed matter physics. As of today, the continuous-time quantum Monte Carlo (CT-QMC)[4] method is the workhorse for obtaining numerical solutions in terms of one- and two-particle Green's functions.

CT-QMC algorithms are based on a stochastic sampling of the diagrammatic series expansion of either the partition function or, directly, the thermal expectation value of some operators, which is also known as worm sampling.[5, 6] For the AIM, one distinguishes between weak coupling expansions in the interaction CT-INT[7] (and related CT-AUX[8]) and strong coupling expansions in the hybridization CT-HYB.[9] While traditionally the former are employed for single-orbital impurity model calculations and impurity clusters, the latter are primarily used for multi-orbital impurity models. The reason for this is that in weak coupling, the exponential scaling of the sign problem makes multi-orbital calculations with non-density-density interactions difficult, while in strong coupling, the exponential scaling of the local Hamiltonian dimensions forbids medium- to large scale clusters.

Conceptually one might expect CT-INT and CT-HYB to behave similarly apart from their differences in scaling with interaction and hybridization strength, respectively. The estimators for one- and two-particle Green's functions are instead considerably different in weak- and strong coupling approaches. While Green's function estimators in CT-INT are formulated as corrections to the non-interacting Green's function[10], this is

not the case for CT-HYB. This results in poor asymptotic behavior of derived quantities, which in turn triggered a series of developments in the CT-HYB community attempting to remedy this problem. These developments include orthogonal polynomial representations as effective low-pass filters[11], moment expansions in the one-particle self-energy[12, 13], asymptotic expressions for the two-particle vertex functions[14, 15] and approaches based on the equation of motion (EOM), often referred to as improved estimators[16–18]. Similar to CT-INT, the improved estimators of CT-HYB calculate the Green's function as a correction to the non-interacting Green's function.

In this paper we introduce and explore the concept of symmetric improved estimators. That is, we derive EOMs by differentiating with respect to all time arguments. The derived equations relate the one- and two-particle Green's function to correlation functions of higher order in the number of creation and annihilation operators. These EOMs may prove useful in various contexts. We employ them for CT-HYB estimators of the self-energy, two-particle (four-leg) and three-leg vertex. We give theoretical arguments showing that the symmetric improved estimators have a strongly reduced noise level at large Matsubara frequencies ν , and even a different scaling with ν , which is confirmed in actual CT-HYB calculations.

Section II introduces the AIM Hamiltonian and our notation for the one- and two-particle Green's function. Section III sketches the derivations for the symmetric improved estimators on the one- and two-particle level. We note that the expressions are based on hierarchies of EOMs and are also useful outside the context of CT-QMC.[19, 20] We further discuss the improved Monte Carlo error scaling of Green's functions, self-energies and vertex functions at large Matsubara frequencies. Section IV discusses the implementation of the symmetric improved estimators in CT-HYB. An implementation for density-density interactions in segment CT-HYB[21] is

* These two authors contributed equally.

straight-forward, an implementation for general interactions requires worm sampling. We discuss drawbacks for a classical worm sampling implementation and propose methods to increase the sampling efficiency. In Section V we show results for self-energies as well as three- and four-leg vertex functions and validate them by comparing to results from exact diagonalization (ED). Finally, Section VI summarizes our work. We furthermore provide an appendix that contains the derivation of the presented formulas in more detail.

II. DEFINITIONS AND MODEL

The AIM consists of an impurity site that is coupled to a bath and its Hamiltonian reads

$$H_{\text{AIM}} = \frac{1}{2} \sum_{ijkl} U_{ijkl} d_i^\dagger d_j^\dagger d_l d_k + \sum_i \tilde{\varepsilon}_i d_i^\dagger d_i + \sum_{Ki} \varepsilon_{Ki} c_{Ki}^\dagger c_{Ki} + \sum_{Kij} \left[V_K^{ij} c_{Ki}^\dagger d_j + (V_K^{ji})^* d_i^\dagger c_{Kj} \right]. \quad (1)$$

Here, d_i (d_i^\dagger) is the annihilation (creation) operator of an electron with spin-orbital flavor i on the impurity; c_{Ki} (c_{Ki}^\dagger) is the annihilation (creation) operator of an electron with impurity flavor i in the non-interacting bath and K subsumes the remaining bath degrees of freedom (e. g. the momentum \mathbf{k}). The impurity is described by a local one-particle potential $\tilde{\varepsilon}_i$ (e.g. the crystal field), the interaction matrix U_{ijkl} , the bath dispersion ε_{Ki} , and the hybridization strength V_K^{ij} . Since the bath degrees of freedom appear in Eq. (1) at most quadratically, they can be formally integrated out yielding a one-body term in the impurity operators. This contains the hybridization function $\Delta_{ab}(\tau_1, \tau_2)$ encoding the entire influence of the bath. In the following we assume a diagonal hybridization $\Delta_{ab}(\tau_1, \tau_2) \equiv \Delta_a(\tau_1, \tau_2) \delta_{ab}$ resulting in a diagonal one-particle Green's function $G_{ab}^{\tau_1 \tau_2} = G_a^{\tau_1 \tau_2} \delta_{ab}$. But the same concept of symmetric improved estimator equations can be extended straight-forwardly to non-diagonal hybridizations.

The hybridization function is most conveniently written in Matsubara frequencies as

$$\Delta_a^\nu = \sum_K \frac{V_K^{aa} (V_K^{aa})^*}{i\nu - \varepsilon_{Ka}}, \quad (2)$$

and it relates to the non-interacting Green's function of the impurity as

$$\mathcal{G}_a^\nu = \frac{1}{i\nu - \tilde{\varepsilon}_a - \Delta_a^\nu}. \quad (3)$$

We define the interacting one-particle Green's function of the AIM as

$$G_a(\tau_1, \tau_2) = -\langle T_\tau d_a(\tau_1) d_a^\dagger(\tau_2) \rangle, \quad (4)$$

where $d_a(\tau)$ ($d_a^\dagger(\tau)$) are now the annihilation (creation) operators for electrons of flavor a at (imaginary) time τ .

Furthermore, T_τ is the imaginary-time ordering operator, and $\langle \dots \rangle = (\text{Tre}^{-\beta H} \dots) / Z$ the thermal expectation value at temperature T ($\beta = 1/T$), Z is the partition function. The Green's function is related to the density as $n_a \equiv \langle d_a^\dagger d_a \rangle = 1 + G_a(0+, 0)$.

Analogously, we define the two-particle Green's function of the AIM as

$$G_{abcd}(\tau_1, \tau_2, \tau_3, \tau_4) = \langle T_\tau d_a(\tau_1) d_b^\dagger(\tau_2) d_c(\tau_3) d_d^\dagger(\tau_4) \rangle. \quad (5)$$

The Fourier transforms to fermionic Matsubara frequencies[22] $\nu = (2l + 1)\pi/\beta$ at integer numbers l are given by

$$G_a^\nu = \frac{1}{\beta} \int_0^\beta d\tau_1 d\tau_2 e^{i\nu(\tau_1 - \tau_2)} G_a(\tau_1, \tau_2) \quad (6)$$

and

$$G_{abcd}^{\nu_1 \nu_2 \nu_3 \nu_4} = \frac{1}{\beta^2} \int_0^\beta d\tau_1 d\tau_2 d\tau_3 d\tau_4 e^{i(\nu_1 \tau_1 - \nu_2 \tau_2 + \nu_3 \tau_3 - \nu_4 \tau_4)} G_{abcd}(\tau_1, \tau_2, \tau_3, \tau_4) \quad (7)$$

for the one- and two-particle Green's function, respectively.

The time translation symmetry of H_{AIM} results in time translation symmetry of Green's functions in imaginary time. This is equivalent to energy conservation, which for the two-particle Green's function reads

$$\nu_1 + \nu_3 = \nu_2 + \nu_4. \quad (8)$$

For the two-particle Green's function it is more common to assume a mixed bosonic-fermionic frequency representation with two fermionic- and one bosonic frequency. However, the choice of these frequencies is ambiguous and therefore the derivations of this paper are done in four fermionic frequencies. With the definitions above, the reader can easily adapt the results to their favorite convention. (Sometimes we use generic bosonic frequencies ω which are however replaced by $\nu_1 \dots \nu_4$ in the final expression.)

III. SYMMETRIC IMPROVED ESTIMATORS

A. One-particle estimator

It is well-known that the Heisenberg equation of motion for a one-particle Green's function is an equation that connects the one- and two-particle Green's functions. This has been exploited in the CT-HYB[16–18] and numerical renormalization group (NRG)[23] algorithms. It leads to the so-called ‘‘improved estimator’’ equation

$$G_a^\nu = \mathcal{G}_a^\nu (1 + \xi_a^\nu), \quad (9)$$

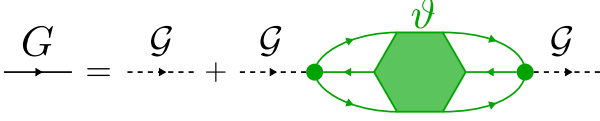


FIG. 1. Feynman-diagrammatic visualization of the symmetric improved estimator Eq. (13) for the one-particle Green's function. The part of the diagram that is drawn in green, will be computed by CT-QMC in the following. Solid lines are full one-particle Green's functions G , dashed lines are non-interacting Green's functions \mathcal{G} , and dots are U -matrices. The three-particle Green's function is represented by the hexagon. Note that the Hartree-term $\propto \sum_j U_{[aj][aj]} n_j$ is excluded.

where

$$\xi_{ab}^\nu = \xi_a^\nu \delta_{ab} = \frac{1}{\beta} \int_0^\beta d\tau_1 d\tau_2 \underbrace{\langle -T_\tau q_a(\tau_1) q_b^\dagger(\tau_2) \rangle}_{\equiv \xi_a(\tau_1, \tau_2)} e^{i\nu(\tau_1 - \tau_2)} \quad (10)$$

is a two-particle Green's function and q contracts three operators at equal time,[24] i.e.,

$$q_a = \sum_{jkl} U_{[aj]kl} d_j^\dagger d_l d_k, \quad (11)$$

$$q_a^\dagger = \sum_{mno} U_{mn[ao]} d_m^\dagger d_n^\dagger d_o. \quad (12)$$

The explicit derivation of this equation of motion can be found in Appendix A and is based on the derivative with respect to the first time argument of G_a .

In this paper, we now express $\xi_a(\tau_1, \tau_2)$ by using the equation of motion again. This time, we apply it to the second time argument of $\xi_a(\tau_1, \tau_2)$, insert it into Eq. (9), and finally arrive at (for the detailed calculation see Appendix A)

$$G_a^\nu = \mathcal{G}_a^\nu \left(1 + \mathcal{G}_a^\nu \left(2 \sum_j U_{[aj][aj]} n_j + \vartheta_a^\nu \right) \right), \quad (13)$$

which is also shown by Feynman diagrams in Fig. 1. Here, we make use of the anti-symmetric U -matrix Eq. (A8) in Appendix A

$$\frac{1}{2} (U_{ijkl} - U_{jikl}) =: U_{[ij]kl} \quad (14)$$

$$\frac{1}{2} (U_{ijkl} - U_{ijlk}) =: U_{ij[kl]}. \quad (15)$$

and the following three-particle Green's function with only two distinct time arguments is employed

$$\vartheta_{ab}^\nu = \vartheta_a^\nu \delta_{ab} = -\frac{1}{\beta} \int_0^\beta d\tau_1 d\tau_2 \langle T_\tau q_a(\tau_1) q_b^\dagger(\tau_2) \rangle e^{i\nu(\tau_1 - \tau_2)}. \quad (16)$$

Error propagation. The declared goal of improved estimators is to reduce high-frequency noise in the quantity of interest. Among one-particle quantities, noise is most prominent in the self-energy. Using Eq. (13) and the Dyson equation, we get

$$\Sigma_a^\nu = \frac{2 \sum_j U_{[aj][aj]} n_j + \vartheta_a^\nu}{1 + \mathcal{G}_a^\nu (2 \sum_j U_{[aj][aj]} n_j + \vartheta_a^\nu)}. \quad (17)$$

The variance of the self-energy can hence approximately be computed by error propagation as (neglecting the error in the density n_i):

$$\text{var}[\Sigma] = \left| \frac{\partial \Sigma}{\partial \vartheta} \right|^2 \text{var}[\vartheta]. \quad (18)$$

Since the derivative goes to 1 in the limit of high frequencies, we conclude that the high-frequency noise amplitude is indeed identical to the noise amplitude of the estimator ϑ_a^ν , which should be independent of ν for large ν . This result for the symmetric improved estimator can be compared to the behavior of the conventional improved estimator for which a discussion of the error propagation can be found elsewhere.[25] The main result is that the error of the conventional improved estimator grows linearly with ν .

B. Two-particle estimator

For the symmetric improved estimator of the two-particle Green's function, we obtain (again see the Appendix B for the derivation):

$$G_{abcd}^{\nu_1 \nu_2 \nu_3 \nu_4} = \mathcal{G}_a^{\nu_1} \left(-R_{1,abcd}^{\nu_1 \nu_2 \nu_3 \nu_4} + \mathcal{G}_b^{\nu_2} \left(R_{2,abcd}^{\nu_1 \nu_2 \nu_3 \nu_4} + \mathcal{G}_c^{\nu_3} \left(-R_{3,abcd}^{\nu_1 \nu_2 \nu_3 \nu_4} + \mathcal{G}_d^{\nu_4} \left(R_{4,abcd}^{\nu_1 \nu_2 \nu_3 \nu_4} + h_{abcd}^{\nu_1 \nu_2 \nu_3 \nu_4} / \beta \right) \right) \right) \right) \text{ where} \quad (19)$$

Name	Formula
ξ_{ab}^ν	$-\int_0^\beta d\tau_1 d\tau_2 \langle T_\tau q_a(\tau_1) d_b^\dagger(\tau_2) \rangle e^{i\nu(\tau_1-\tau_2)} / \beta$
ϑ_{ab}^ν	$-\int_0^\beta d\tau_1 d\tau_2 \langle T_\tau q_a(\tau_1) q_b^\dagger(\tau_2) \rangle e^{i\nu(\tau_1-\tau_2)} / \beta$
ϕ_{abcd}^ω	$\int d\tau_1 d\tau_2 \langle T_\tau (Un)_{ab}(\tau_1) (Un)_{cd}(\tau_2) \rangle e^{i\omega(\tau_1-\tau_2)} / \beta$
ψ_{abcd}^ω	$\int d\tau_1 d\tau_2 \langle T_\tau (Udd)_{ac}(\tau_1) (Ud^\dagger d^\dagger)_{bd}(\tau_2) \rangle e^{i\omega(\tau_1-\tau_2)} / \beta$
$f_{abcd}^{\nu\omega}$	$\int d\tau_1 d\tau_2 d\tau_3 \langle T_\tau q_a(\tau_1) q_b^\dagger(\tau_2) (Un)_{cd}(\tau_3) \rangle e^{i\nu(\tau_1-\tau_2)+i\omega(\tau_2-\tau_3)} / \beta$
$g_{abcd}^{\nu\nu'}$	$\int d\tau_1 d\tau_2 d\tau_3 \langle T_\tau q_a(\tau_1) q_c(\tau_2) (Ud^\dagger d^\dagger)_{bd}(\tau_3) \rangle e^{i\nu(\tau_1-\tau_3)+i\nu'(\tau_2-\tau_3)} / \beta$
$h_{abcd}^{\nu_1\nu_2\nu_3\nu_4}$	$\int d\tau_1 d\tau_2 d\tau_3 d\tau_4 \langle T_\tau q_a(\tau_1) q_b^\dagger(\tau_2) q_c(\tau_3) q_d^\dagger(\tau_4) \rangle e^{i(\nu_1\tau_1-\nu_2\tau_2+\nu_3\tau_3-\nu_4\tau_4)} / \beta$

TABLE I. Terms of the symmetric improved estimators. We use the abbreviations $(Un)_{ab} = \sum_{jk} U_{[aj][bk]} d_j^\dagger d_k$, $(Ud^\dagger d^\dagger)_{ab} = \sum_{jk} U_{jk[ab]} d_j^\dagger d_k^\dagger$ and $(Udd)_{ab} = \sum_{jk} U_{[ab]jk} d_k d_j$. Frequencies $\nu_{(i)}$ and ω are fermionic and bosonic Matsubara frequencies, respectively.

$$R_1^{\nu_1\nu_2\nu_3\nu_4} = -\delta_{12} G_d^{\nu_4} + \delta_{14} G_b^{\nu_2}, \quad (20)$$

$$R_2^{\nu_1\nu_2\nu_3\nu_4} = -\delta_{12} \mathcal{G}_c^{\nu_3} 2 \sum_j U_{[aj][aj]} n_j - \delta_{14} \xi_d^{\nu_4} - \frac{2}{\beta} \mathcal{G}_c^{\nu_3} \mathcal{G}_d^{\nu_4} \left[-U_{[ac][bd]} + \sum_i \left(U_{[ai][bd]} \xi_{ci}^{\nu_3} + U_{[ac][bi]} \xi_{di}^{\nu_4} \right) - 2\phi_{abcd}^{\nu_4-\nu_3} + f_{cdab}^{\nu_3(\nu_3-\nu_4)} \right], \quad (21)$$

$$R_3^{\nu_1\nu_2\nu_3\nu_4} = \delta_{12} \vartheta_a^{\nu_1} + \frac{1}{\beta} \mathcal{G}_d^{\nu_4} \left[2 \sum_i \left(U_{[ic][bd]} \xi_{ai}^{\nu_1} + U_{[ac][id]} \xi_{bi}^{\nu_2} \right) - \psi_{abcd}^{\nu_1+\nu_3} + 4\phi_{adcb}^{\nu_1-\nu_4} + 2f_{adcb}^{\nu_1(\nu_1-\nu_4)} - g_{dcb a}^{\nu_4\nu_2} \right], \quad (22)$$

$$R_4^{\nu_1\nu_2\nu_3\nu_4} = \frac{1}{\beta} \left[2f_{cbad}^{\nu_3(\nu_4-\nu_1)} + g_{abcd}^{\nu_1\nu_3} - 2f_{abcd}^{\nu_1(\nu_1-\nu_2)} \right]. \quad (23)$$

All estimators occurring on the right-hand side of Eqs. (20)-(23) are defined in Table I. In order to obtain a more symmetric form, we further made use of the relations $\delta_{\nu_1\nu_2} \equiv \delta_{\nu_1\nu_2} \delta_{\nu_3\nu_4}$ and $\delta_{\nu_1\nu_4} \equiv \delta_{\nu_2\nu_3} \delta_{\nu_3\nu_4}$, which are valid due to energy conservation. Additionally we em-

ployed $\delta_{12} \equiv \delta_{ab} \delta_{cd} \delta_{\nu_1\nu_2} \delta_{\nu_3\nu_4}$ and $\delta_{14} \equiv \delta_{ad} \delta_{bc} \delta_{\nu_1\nu_4} \delta_{\nu_2\nu_3}$ to make the expressions shorter.

Inserting the R_i terms from Eqs. (20)-(23) into Eq. (19) and regrouping the terms leads to the following expression for the symmetric improved two-particle Green's function:

$$G_{abcd}^{\nu_1\nu_2\nu_3\nu_4} = (\delta_{12} - \delta_{14}) G_a^{\nu_1} G_c^{\nu_3} - \frac{1}{\beta} \mathcal{G}_a^{\nu_1} \mathcal{G}_b^{\nu_2} \mathcal{G}_c^{\nu_3} \mathcal{G}_d^{\nu_4} \mathfrak{F}_{abcd}^{\nu_1\nu_2\nu_3\nu_4} \quad \text{with}$$

$$\mathfrak{F}_{abcd}^{\nu_1\nu_2\nu_3\nu_4} = \beta (\delta_{12} - \delta_{14}) \left(2 \sum_i U_{[ai][ai]} n_i + \vartheta_a^{\nu_1} \right) \left(2 \sum_j U_{[cj][cj]} n_j + \vartheta_c^{\nu_3} \right) + 2U_{[ac][bd]} + 2 \sum_i \left(U_{[ic][bd]} \xi_{ai}^{\nu_1} + U_{[ac][id]} \xi_{bi}^{\nu_2} + U_{[ai][bd]} \xi_{ci}^{\nu_3} + U_{[ac][bi]} \xi_{di}^{\nu_4} \right) - \underbrace{4\phi_{abcd}^{\nu_1-\nu_2} + 2f_{abcd}^{\nu_1(\nu_1-\nu_2)} + 2f_{cdab}^{\nu_3(\nu_2-\nu_1)}}_{(i)} + \underbrace{4\phi_{adcb}^{\nu_1-\nu_4} - 2f_{adcb}^{\nu_1(\nu_1-\nu_4)} - 2f_{cbad}^{\nu_3(\nu_4-\nu_1)}}_{(ii)} - \underbrace{\psi_{abcd}^{\nu_1+\nu_3} - g_{abcd}^{\nu_1\nu_3} - g_{dcb a}^{\nu_4\nu_2}}_{(iii)} + h_{abcd}^{\nu_1\nu_2\nu_3\nu_4}. \quad (24)$$

(A pictorial representation of this formula is found in Fig. 2.) The quantities entering here are the anti-symmetrized Coulomb interaction U , the one-particle density n_i and the correlators ϑ and ξ which already appeared for the one-particle Green's function in Section III A. In order to shorten the expression, we singled

out the disconnected part $(\delta_{12} - \delta_{14}) G_a^{\nu_1} G_c^{\nu_3}$ of the two-particle Green's function by applying Eq. (13). However, there remains another term proportional to $(\delta_{12} - \delta_{14})$ in \mathfrak{F} . This is rooted in the expansion via equations of motion, which always leads to expressions involving non-interacting Green's functions \mathcal{G} . The 10 terms in

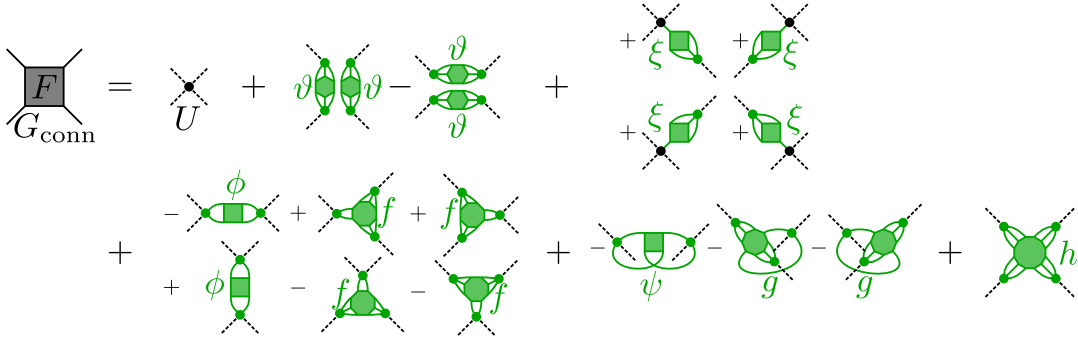


FIG. 2. Heuristic drawing of the Feynman-diagrammatic decomposition of the connected part of the two-particle Green's function, as obtained by symmetric improved estimators. The estimators that are later computed by CT-QMC are drawn in green. Solid lines represent interacting one-particle Green's functions G , dashed lines are non-interacting Green's functions \mathcal{G} , and dots are U -matrices. The terms involving ϑ are to be understood as products. Note that Hartree-like terms and products thereof are not shown, in order to make the picture more concise.

the last line of Eq. (24) are genuinely related to the two-particle Green's function. Further, the frequency structure of the terms (i)-(iii) resembles the contributions from the particle-hole, transversal particle-hole and particle-particle channel [26]. The last term $h_{abcd}^{\nu_1\nu_2\nu_3\nu_4}$ must hence include fully irreducible contributions.

Two-particle vertex. As for two-particle quantities, one is often interested in vertex functions instead of the Green's function itself, e.g. when calculating susceptibilities [27, 28] or for diagrammatic extensions of DMFT [26, 29, 30]. The full vertex F is related to the two-particle Green's function by

$$G_{abcd}^{\nu_1\nu_2\nu_3\nu_4} = (\delta_{12} - \delta_{14})G_a^{\nu_1}G_c^{\nu_3} - \frac{1}{\beta}G_a^{\nu_1}G_b^{\nu_2}G_c^{\nu_3}G_d^{\nu_4}F_{abcd}^{\nu_1\nu_2\nu_3\nu_4}. \quad (25)$$

This bears a certain similarity to Eq. (24), and it becomes apparent, that the full vertex is given by

$$F_{abcd}^{\nu_1\nu_2\nu_3\nu_4} = \frac{\mathcal{G}_a^{\nu_1}\mathcal{G}_b^{\nu_2}\mathcal{G}_c^{\nu_3}\mathcal{G}_d^{\nu_4}}{G_a^{\nu_1}G_b^{\nu_2}G_c^{\nu_3}G_d^{\nu_4}}\mathfrak{F}_{abcd}^{\nu_1\nu_2\nu_3\nu_4}. \quad (26)$$

Error propagation. Assuming that quantities measured in CT-QMC have approximately the same noise amplitude over the whole frequency range, we can conclude that this holds for \mathfrak{F} as well. We furthermore conclude from Eq. (26) that the noise amplitude is rescaled by \mathcal{G}^ν/G^ν in every frequency variable. Since this ratio goes to 1 in the limit of high frequency, we may finally conclude that the noise amplitude of the vertex F in the high-frequency region is identical to the noise amplitude of \mathfrak{F} and thus directly proportional to the error of the Monte Carlo simulation. We hence expect (and will confirm this later) a constant noise level for large Matsubara frequencies.

In contrast, for conventional CT-QMC calculations in the hybridization expansion a strong increase of noise in F with increasing Matsubara frequencies is observed. This yields a too noisy vertex at high frequencies so that approaches to circumvent the calculation of F at large

frequencies have been developed, as e.g. replacing the vertex by its high frequency asymptotics [15]. This high noise level of conventional CT-HYB calculations can be understood from Eq. (25). If we assume a constant noise level of the two-particle Green's function on the left hand side, extracting F by dividing through four Green's functions increases the error four times by a factor $\sim \nu_i$ for large ν_i .

C. Three-leg vertex

Let us further define the particle-hole three-leg Green's function as

$$G_{abcd}^{\nu_1\nu_2} = \frac{1}{\beta} \int_0^\beta d\tau_1 d\tau_2 d\tau_3 e^{i\nu_1(\tau_1 - \tau_3) - i\nu_2(\tau_2 - \tau_3)} \times \langle T_\tau d_a(\tau_1) d_b^\dagger(\tau_2) [d_c d_d^\dagger](\tau_3) \rangle, \quad (27)$$

where ν_1 and ν_2 are fermionic Matsubara frequencies. Differentiation with respect to τ_1 and τ_2 leads to the symmetric improved version

$$G_{abcd}^{\nu_1\nu_2} = -\beta\delta_{12}(1 - n_c)G_a^{\nu_1} - \delta_{14}G_a^{\nu_1}G_b^{\nu_2} - \mathcal{G}_a^{\nu_1}\mathcal{G}_b^{\nu_2} [\beta\delta_{12}n_c(2(Un)_a + \vartheta_a^{\nu_1}) - \delta_{14}\xi_a^{\nu_1}\xi_b^{\nu_2} - 2\hat{\phi}_{abcd}^{\nu_1-\nu_2} + \hat{f}_{abcd}^{\nu_1(\nu_1-\nu_2)}], \quad (28)$$

with the auxiliary definitions

$$\hat{\phi}_{abcd}^\omega = \frac{1}{\beta} \int d\tau_1 d\tau_2 e^{i\omega(\tau_1 - \tau_2)} \langle T_\tau \sum_{jk} U_{[aj][bk]} [d_j^\dagger d_k](\tau_1) [d_d^\dagger d_c](\tau_2) \rangle \quad (29)$$

and

$$\hat{f}_{abcd}^{\nu\omega} = \frac{1}{\beta} \int d\tau_1 d\tau_2 d\tau_3 e^{i\nu(\tau_1 - \tau_2) + i\omega(\tau_2 - \tau_3)} \langle T_\tau q_a(\tau_1) q_b^\dagger(\tau_2) [d_d^\dagger d_c](\tau_3) \rangle. \quad (30)$$

Since the R_2 term of the symmetric improved estimator of the two-particle Green's function essentially contains a threeleg Green's function, the derivation of the threeleg symmetric improved estimator is completely analogous to the one shown in the last subsection of Appendix B.

For diagrammatic extensions of DMFT, the associated three-leg vertex functions are often particularly interesting, see e.g. Refs. [31–35]. These are related to the three-leg Green's function by subtraction of disconnected parts and division by two one-particle Green's functions. Representative for the variety of definitions, we show the so-called Kernel-2 function in the particle-hole channel (for a definition see [14, 15, 36]), which can be obtained through the following symmetric improved estimator

$$K_{abcd}^{(2),ph,\nu_1\nu_2} = (4\beta\delta_{12}(Un)_a(Un)_c - 4\phi_{abcd}^{\nu_1-\nu_2}) \left(\frac{G_a^{\nu_1} G_b^{\nu_2}}{G_a^{\nu_1} G_b^{\nu_2}} - 1 \right) + 2 \frac{G_a^{\nu_1} G_b^{\nu_2}}{G_a^{\nu_1} G_b^{\nu_2}} [\beta\delta_{12}\vartheta_a^{\nu_1}(Un)_c - \xi_a^{\nu_1} \xi_b^{\nu_2} U_{[cb][da]} + f_{abcd}^{\nu_1(\nu_1-\nu_2)}]. \quad (31)$$

IV. IMPLEMENTATION

As discussed before, the expressions for e.g. the one- or two-particle Green's functions derived using the EOM (Eq. (13) and Eq. (24)) can be employed in a CT-HYB simulation to obtain results with asymptotically smaller error for high frequencies. In the simulation, we need to get the QMC estimates for the values of each individual term contributing to the symmetric improved estimators (cf. Tab. I), i.e. of correlation functions consisting of up to 12 operators with up to 4 different imaginary time or 3 different Matsubara frequency arguments with several components corresponding to possible combinations of the discrete quantum numbers of the operators. We accomplish this by performing worm sampling in our CT-HYB w2DYNAMICS[37] program package.

A full introduction to the CT-HYB algorithm is given in Ref. 4, but for the sake of understanding let us briefly recall some main aspects. The starting point is the AIM Hamiltonian Eq. (1). After integrating out the bath degrees of freedom one can evaluate the thermodynamic partition function $Z = \text{Tr} \exp(-\beta H)$ for the impurity by summing over all impurity field configurations. The CT-HYB choice of expanding the exponential in the hybridization turns it into a series of “local” traces. These consist of pairs of impurity operators that evolve in imaginary time according to the local part of the Hamiltonian. The hybridization with the bath is described by a determinant of a matrix that contains, order by order, the hybridization function Δ where the impurity operators in the local trace are.

Each combination of expansion order, imaginary times, orbitals and spins of the local operators describes one point in the space of partition function configurations \mathcal{C}_Z . The quantity of interest, e.g. a Green's function $G_{ab} = \text{Tr} T_\tau \exp(-\beta H) d_a(\tau_a) d_b^\dagger(\tau_b) / Z$, can be obtained from \mathcal{C}_Z

either by manipulating a \mathcal{C}_Z configuration accordingly in the measurement step or by directly sampling $\mathcal{C}_{G_{ab}}$ configurations. These are like the \mathcal{C}_Z configurations, but explicitly contain (in this case) two additional operators (“worm”) that appear in the definition of G_{ab} . The worm algorithm consists in sampling both $\mathcal{C}_{G_{ab}}$ and \mathcal{C}_Z (for normalization) in one simulation. More details on worm sampling can be found in Ref. 6.

This kind of worm sampling is employed for the calculation of each component $k_{a_1 \dots a_n}$ of each correlation function k needed for the symmetric improved estimator (see Table I). When we perform a sampling run in the extended configuration space $\mathcal{C}_Z \oplus \mathcal{C}_{k_{a_1 \dots a_n}}$ which includes partition function configurations and worm configurations for the specific correlation function, the measurement procedure itself trivially consists of counting samples.

As we have seen, the weight in the worm spaces differs from the weight of a similar Z space configuration in the value of the local trace, but we also explicitly add a suitably chosen weight factor $\eta_{k_{a_1 \dots a_n}}$ to balance the number of steps spent in the current worm space and the partition function space. It is not necessary to perform separate runs per component and quantity, but this also makes it simpler in practice to select the appropriate amount of measurements for the desired target error of the final result (to which all components of all quantities may contribute differently).

In both configuration spaces, we allow all moves that only change operators connected to hybridization events, i.e. in our case pair insertions, pair removals and some global moves. Additionally, worm insertion and removal steps must be employed to change between the two subspaces \mathcal{C}_Z and $\mathcal{C}_{k_{a_1 \dots a_n}}$. For estimators with density-like parts only, such as ϕ_{aabb}^ω , this should even in practice be enough to ensure ergodic sampling. For other estimators, possible quantum number violations (i.e. configurations with two sequential operators that are zero because of commutation relations) and changes in the energies of states occurring in the local time evolution strongly suppress insertions with large time differences between “compensating” operators (cf. Ref. 6 and 38). If the worm operators' positions could only be changed in the worm insertion step, this would lead to problematically bad statistics for large distances (towards $\Delta\tau = \beta/2$).

Therefore, we introduce further moves that shift or replace some of the estimator's worm operators analogous to the worm replacement moves[6]. In Ref. 6, these moves transfer the “worm status” from a worm operator to a hybridization operator, i.e. they change which operators are connected with hybridization events (and accordingly only change the bath weight). Since, contrary to Ref. 6, our estimators contain several operators at equal times, the procedure needs to be slightly modified as compared to a simple replacement: After we select one impurity operator connected to a hybridization event at τ_h and one worm operator at τ_w for a replacement, we not only “exchange” them (changing only the bath part of the

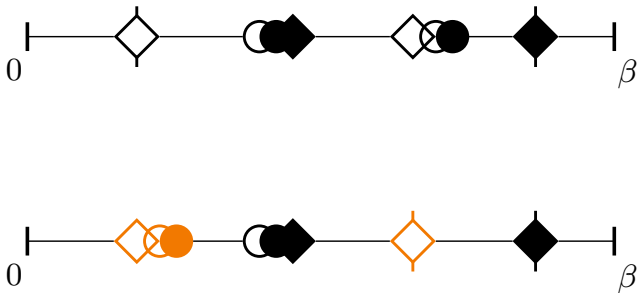


FIG. 3. Symbolic representation of a “replacement” move applied to a worm operator that is at equal time with two other operators. Operators are represented as symbols (flavors) on the imaginary time axis before (top) and after (bottom) the move, with filled symbols representing creators and little vertical tags at the symbols’ top and bottom signifying operators connected to hybridization events. Changes due to the move are marked in orange.

weight), but also move any other worm operators at τ_w to τ_h to reconstruct the same equal-time object at another position (cf. Fig. 3). This may cause a lower acceptance rate compared to simpler replacements, but especially if the other worm operators are density-like (which may e.g. be the case when performed on a q), these moves are reasonably effective.

V. VALIDATION

The best way to validate CT-QMC results is benchmarking against exact diagonalization (ED). To this end CT-QMC results were calculated in w2DYNAMICS[37] and, at the same time, all estimators were calculated exactly by evaluating their Lehmann representation for a small Hamiltonian, i.e. an impurity model with one orbital and a discrete bath. The ED results were also used to confirm the validity of Eq. (24).

Specifically, we choose a bath with one energy level $\varepsilon_{\text{bath}} = 0.5$ and hybridization amplitude $V = 0.3$. The chemical potential is set to $\mu = -0.1$, the inverse temperature is chosen to be $\beta = 10$ and the local interaction $U = 2$. At these parameters, every spin-orbital is on average occupied by 0.307 electrons.

A. Self-energy

The quantities G^ν , ξ^ν and θ^ν were evaluated by performing 1.44×10^9 QMC measurements on their respective estimators. Subsequently the one-particle Green’s function and the self-energy were calculated from Eq. (9) and Eq. (13). Fig. 4 shows a comparison of the improved and the symmetric improved self-energy as well as the one obtained directly from the CT-HYB Green’s function as calculated by worm sampling without improved estimators. We note that both “improved” ways

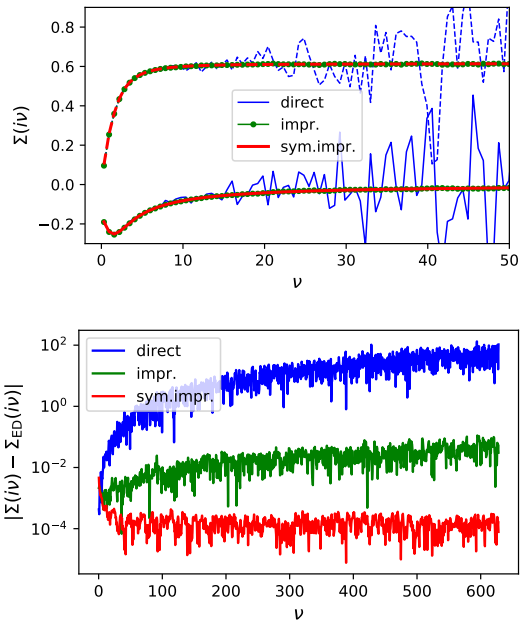


FIG. 4. Upper panel: Comparison of the self-energy (for the AIM specified in Sec. V), as calculated from the directly measured one-particle Green’s function (*direct*) vs. the result obtained with improved (*impr.*) and symmetrically improved (*sym. impr.*) estimators. Lower panel: logplot of the absolute difference to exact diagonalization data.

to calculate the self-energy suffer from lower precision in the low-frequency regime. However, except for the first few Matsubara frequencies, where precise quantities can be obtained by conventional Z -sampling of the Green’s function, the symmetric improved one-particle estimator yields considerably better results. As anticipated in Section III A, we also observe a better scaling of the error at high Matsubara frequencies.

B. Vertex functions

Vertex functions are related to the two-particle Green’s function. In order to assemble the symmetric improved form by Eq. (24), one needs to sample all seven occurring estimators. The full vertex $F^{\nu\nu'\omega} \equiv F^{\nu(\nu-\omega)(\nu'-\omega)\nu'}$ can be obtained from the connected part of the two-particle Green’s function by “amputation” of its legs, i. e. division by a product of four Green’s functions, cf. Eq. (25). In the high-frequency case this leads to massive noise amplification, if the two-particle Green’s function is directly computed in QMC. However, as discussed in Sec. III B, this is healed by symmetric improved estimators. In Fig. 5 we show slices through $F_{\uparrow\uparrow\downarrow\downarrow}^{\nu\nu'\omega}$ at two fixed bosonic frequencies ω . In analogy to the one-particle estimator, we get precise results over the whole frequency range, and in particular, there is no increase of noise at high Matsubara frequencies.

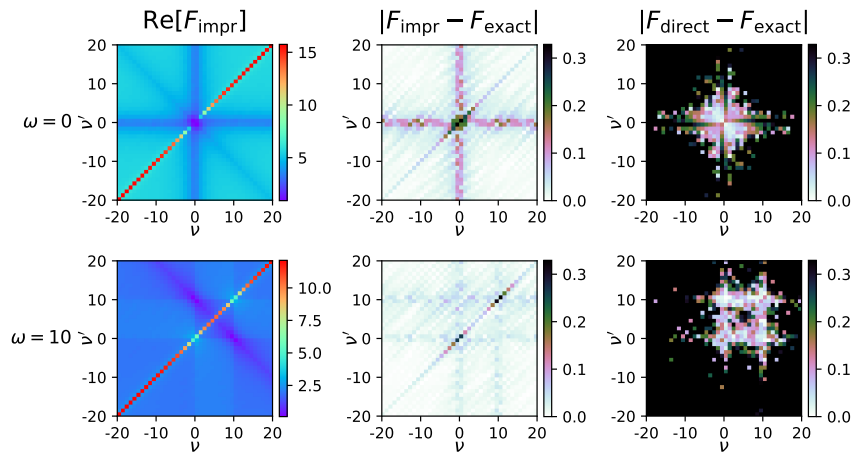


FIG. 5. Reducible vertex $F_{\uparrow\uparrow\downarrow\downarrow}^{\nu\nu'\omega}$. Upper row: bosonic frequency $\nu_1 - \nu_2 = \omega = 0$; lower row: $\nu_1 - \nu_2 = \omega = 10 \times 2\pi/\beta$. First column: F as calculated with symmetric improved estimators; second column: difference of the symmetric improved to the exact result, third column: difference of the conventional calculation (directly measured two-particle Green's function) to the exact result.

C. Three-leg vertex

Eq. (31) allows us to compute the kernel-2 function $K^{(2),ph,\nu(\nu-\omega)}$ from QMC-estimators that were also used for the full two-particle vertex. In order to judge the improvement introduced by Eq. (31), we compute $K_{\uparrow\uparrow\downarrow\downarrow}^{(2),ph,\nu(\nu-\omega)}$ not only in this new way, but also in the way of Ref. 15 from the three-leg Green's function Eq. (27) measured in QMC. In Fig. 6 we compare the result obtained by symmetric improved estimators to the exact result and to the result of the conventional calculation. Notably also here the increase of noise at high Matsubara frequencies is absent.

VI. CONCLUSION

We derived equations of motion for the one- and two-particle Green's function differentiating symmetrically with respect to all time arguments. With these symmetric improved estimators, we found a way to compute self-energy and vertex functions in CT-HYB without suffering from noise that strongly increases at high Matsubara frequencies as in conventional CT-HYB calculations. In fact, our results rapidly converge towards the exact results, with the exception of the lowest few Matsubara frequencies, where our estimators do not lead to an improvement. For very weak hybridization the self-energy and vertex on the lowest few Matsubara frequencies can actually be calculated with higher accuracy if no improved estimators are used. We hence conclude that in some cases it will be best to combine conventional and improved estimators, using the former for small frequencies and the latter at large frequencies.

ACKNOWLEDGMENTS

We thank Markus Wallerberger, Andreas Hausoel, Tin Ribic, Oleg Janson, and Dominique Geffroy for valuable

discussions. This work has been supported by the Vienna Scientific Cluster (VSC) Research Center funded by the Austrian Federal Ministry of Science, Research and Economy (bmwfw), the Deutsche Forschungs Gemeinschaft (DFG) through research unit FOR 1346, the Austrian Science Fund (FWF) through project P 30997-N32, and the European Research Council under the European Union's Seventh Framework Programme (FP/2007-2013)/ERC grant agreement n. 306447 (AbinitioDFA). J.K. was partially supported by the Leibniz society through the Leibniz competition. A.K. and G.S. have been supported by the DFG (through SFB 1170 "ToCoTronics"). G. S. further acknowledges financial support from the DFG through the Würzburg-Dresden Cluster of Excellence on Complexity and Topology in Quantum Matter – *ct.qmat* (EXC 2147, project-id 39085490). Some of the computational results were obtained using the Vienna Scientific Cluster (VSC). The authors also gratefully acknowledge the Gauss Centre for Supercomputing e.V. (www.gauss-centre.eu) for funding this project by providing computing time on the GCS Supercomputer SuperMUC at Leibniz Supercomputing Centre (www.lrz.de).

Appendix A: One-particle Symmetric Improved Estimator

The first-order equations (i.e. improved estimators) were already derived in Ref. 16. We nevertheless give a detailed derivation to introduce notation and concepts necessary to derive higher-order estimators (i.e. symmetric improved estimators) in the following. This further sets the stage for the two-particle symmetric improved estimators.

The time derivative of the one-particle Green's func-

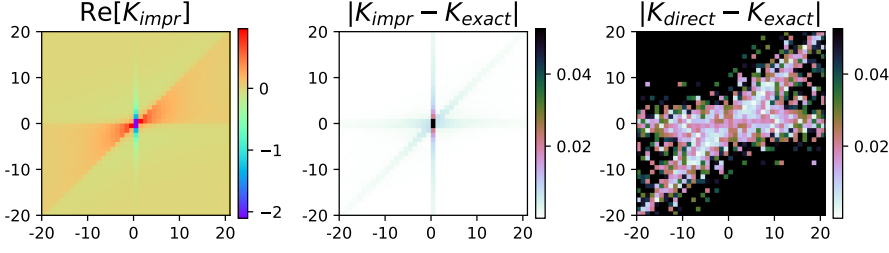


FIG. 6. Three-leg kernel function $K_{\uparrow\uparrow\downarrow}^{(2),ph,\nu(\nu-\omega)}$, calculated by Eq. (31) (left), its difference to the exact result (middle), and the difference of the conventional, direct calculation to the exact result (right).

tion follows as:

$$\partial_{\tau_1} G_a(\tau_1, \tau_2) = -\partial_{\tau_1} \langle T_{\tau} d_a(\tau_1) d_a^{\dagger}(\tau_2) \rangle \quad (\text{A1})$$

$$= -\partial_{\tau_1} (\theta(\tau_1 - \tau_2) \langle d_a(\tau_1) d_a^{\dagger}(\tau_2) \rangle - \theta(\tau_2 - \tau_1) \langle d_a^{\dagger}(\tau_2) d_a(\tau_1) \rangle) \quad (\text{A2})$$

$$= -\delta(\tau_1 - \tau_2) \underbrace{\langle \{d_a, d_a^{\dagger}\}(\tau_1) \rangle}_{=1} - \langle T_{\tau} (\partial_{\tau_1} d_a(\tau_1)) d_a^{\dagger}(\tau_2) \rangle \quad (\text{A3})$$

$$= -\delta(\tau_1 - \tau_2) - \langle T_{\tau} [H_{\text{AIM}}, d_a](\tau_1) d_a^{\dagger}(\tau_2) \rangle. \quad (\text{A4})$$

The commutator between the local Hamiltonian and the impurity-annihilation operator on the right hand side can be calculated as:

$$\begin{aligned} [H_{\text{AIM}}, d_a] &= \frac{1}{2} \sum_{ijkl} U_{ijkl} (d_i^{\dagger} d_j^{\dagger} d_l d_k d_a - d_a d_i^{\dagger} d_j^{\dagger} d_l d_k) \\ &+ \sum_i \tilde{\varepsilon}_i (d_i^{\dagger} d_i d_a - d_a d_i^{\dagger} d_i) \\ &+ \sum_{Ki} (V_K^{ii})^* (d_i^{\dagger} c_{Ki} d_a - d_a d_i^{\dagger} c_{Ki}) \end{aligned} \quad (\text{A5})$$

$$\begin{aligned} &= \frac{1}{2} \sum_{ijkl} U_{ijkl} (d_i^{\dagger} \delta_{aj} d_l d_k - \delta_{ai} d_j^{\dagger} d_l d_k) \\ &- \sum_i \tilde{\varepsilon}_i \delta_{ai} d_i - \sum_{Ki} (V_K^{ii})^* \delta_{ai} c_{Ki} \quad (\text{A6}) \\ &= -\sum_{jkl} U_{[aj]kl} d_j^{\dagger} d_l d_k - \tilde{\varepsilon}_a d_a - \sum_K (V_K^{aa})^* c_{Ka}, \end{aligned} \quad (\text{A7})$$

with hybridization V_K^{aa} and the anti-symmetrizations of the interaction matrix:

$$\frac{1}{2} (U_{ijkl} - U_{jikl}) =: U_{[ij]kl} \quad (\text{A8})$$

$$\frac{1}{2} (U_{ijkl} - U_{ijlk}) =: U_{ij[kl]}. \quad (\text{A9})$$

It is convenient to introduce new operators for the contractions of the interaction matrix with three local operators:

$$q_a = \sum_{jkl} U_{[aj]kl} d_j^{\dagger} d_l d_k \quad (\text{A10})$$

$$q_a^{\dagger} = \sum_{mno} U_{mn[ao]} d_m^{\dagger} d_n^{\dagger} d_o. \quad (\text{A11})$$

With these equal-time three-particle operators, the one-particle Green's function follows as:

$$\begin{aligned} \partial_{\tau_1} G_a(\tau_1, \tau_2) &= -\delta(\tau_1 - \tau_2) + \langle T_{\tau} q_a(\tau_1) d_a^{\dagger}(\tau_2) \rangle \\ &+ \langle T_{\tau} \tilde{\varepsilon}_a d_a(\tau_1) d_a^{\dagger}(\tau_2) \rangle \\ &+ \langle T_{\tau} \sum_K (V_K^{aa})^* c_{Ka}(\tau_1) d_a^{\dagger}(\tau_2) \rangle, \end{aligned} \quad (\text{A12})$$

which is the equation of motion for the impurity Green's function of the AIM.

The mixed impurity-bath Green's function can be further calculated by applying the above procedure onto the bath operator once again:

$$\begin{aligned} \partial_{\tau_1} \langle T_{\tau} c_{Ka}(\tau_1) d_a^{\dagger}(\tau_2) \rangle &= \delta(\tau_1 - \tau_2) \underbrace{\langle \{c_{Ka}, d_a^{\dagger}\}(\tau_1) \rangle}_{=0} \\ &+ \langle T_{\tau} [H_{\text{AIM}}, c_{Ka}](\tau_1) d_a^{\dagger}(\tau_2) \rangle \end{aligned} \quad (\text{A13})$$

Here, the commutator between the local Hamiltonian and the bath-annihilation operator can be calculated as:

$$\begin{aligned} [H_{\text{AIM}}, c_{Ka}] &= \sum_{K'i} \varepsilon_{K'i} (c_{K'i}^{\dagger} c_{K'i} c_{Ka} - c_{Ka} c_{K'i}^{\dagger} c_{K'i}) \\ &+ \sum_{K'i} V_{K'i}^{ii} (c_{K'i}^{\dagger} d_i c_{Ka} - c_{Ka} c_{K'i}^{\dagger} d_i) \quad (\text{A14}) \\ &= -\sum_{K'i} \varepsilon_{K'i} \delta_{KK'} \delta_{ai} c_{K'i} - \sum_{K'i} V_{K'i}^{ii} \delta_{KK'} \delta_{ai} d_i. \end{aligned} \quad (\text{A15})$$

Thus we can relate the time-derivative of the mixed impurity-bath Green's function to the impurity Green's function:

$$(\partial_{\tau_1} + \varepsilon_{Ka}) \langle T_{\tau} c_{Ka}(\tau_1) d_a^{\dagger}(\tau_2) \rangle = -V_K^{aa} \langle T_{\tau} d_a(\tau_1) d_a^{\dagger}(\tau_2) \rangle. \quad (\text{A16})$$

In order to insert this into Eq. (A12), we have to Fourier-transform the above expression with respect to τ_1 :

$$\begin{aligned} &\int_0^{\beta} d\tau_1 e^{i\nu_1 \tau_1} \partial_{\tau_1} \langle T_{\tau} c_{Ka}(\tau_1) d_a^{\dagger}(\tau_2) \rangle \\ &= -\int_0^{\beta} d\tau_1 e^{i\nu_1 \tau_1} (\varepsilon_{Ka} \langle T_{\tau} c_{Ka}(\tau_1) d_a^{\dagger}(\tau_2) \rangle \\ &\quad + V_K^{aa} \langle T_{\tau} d_a(\tau_1) d_a^{\dagger}(\tau_2) \rangle) \end{aligned} \quad (\text{A17})$$

Now the expression on the left-hand side of Eq. (A17) can be simplified by integration by parts and we have

$$\begin{aligned} & \int_0^\beta d\tau_1 e^{i\nu_1 \tau_1} \langle T_\tau c_{Ka}(\tau_1) d_a^\dagger(\tau_2) \rangle \\ &= \frac{V_K^{aa}}{i\nu_1 - \varepsilon_{Ka}} \int_0^\beta d\tau_1 e^{i\nu_1 \tau_1} \langle T_\tau d_a(\tau_1) d_a^\dagger(\tau_2) \rangle \end{aligned} \quad (\text{A18})$$

Applying the same Fourier transform and integration by parts also to Eq. (A12) allows us to insert the above result and we get

$$\begin{aligned} i\nu_1 \int_0^\beta d\tau_1 e^{i\nu_1 \tau_1} \langle T_\tau d_a(\tau_1) d_a^\dagger(\tau_2) \rangle &= - \int_0^\beta d\tau_1 e^{i\nu_1 \tau_1} \delta(\tau_1 - \tau_2) \\ &+ \int_0^\beta d\tau_1 e^{i\nu_1 \tau_1} \langle T_\tau q_a(\tau_1) d_a^\dagger(\tau_2) \rangle \\ &+ \tilde{\varepsilon} \int_0^\beta d\tau_1 e^{i\nu_1 \tau_1} \langle T_\tau d_a(\tau_1) d_a^\dagger(\tau_2) \rangle \\ &+ \underbrace{\sum_K \frac{V_K^{aa} (V_K^{aa})^*}{i\nu_1 - \varepsilon_{Ka}}}_{\Delta_a^{\nu_1}} \int_0^\beta d\tau_1 e^{i\nu_1 \tau_1} \langle T_\tau d_a(\tau_1) d_a^\dagger(\tau_2) \rangle \end{aligned} \quad (\text{A19})$$

Now the terms can be regrouped to express the Green's function:

$$\begin{aligned} & \underbrace{(i\nu_1 - \tilde{\varepsilon}_a - \Delta_a^{\nu_1})}_{[\mathcal{G}_a^{\nu_1}]^{-1}} \int_0^\beta d\tau_1 e^{i\nu_1 \tau_1} \langle T_\tau d_a(\tau_1) d_a^\dagger(\tau_2) \rangle \\ &= - \int_0^\beta d\tau_1 e^{i\nu_1 \tau_1} [\delta(\tau_1 - \tau_2) - \langle T_\tau q_a(\tau_1) d_a^\dagger(\tau_2) \rangle] \end{aligned} \quad (\text{A20})$$

This expression can be Fourier-transformed with respect to τ_2 by applying $\int_0^\beta d\tau_2 \exp(-i\nu_2 \tau_2)$ to both sides of the equation. Considering the definitions of the Green's function and the function ξ , one arrives at Eq. (9).

In order to obtain the symmetric improved estimator, the equal-time two-particle Green's function is differentiated with respect to the impurity creation operator at time τ_2 , such that:

$$\begin{aligned} \partial_{\tau_2} \langle T_\tau q(\tau_1) d_a^\dagger(\tau_2) \rangle &= -\delta(\tau_1 - \tau_2) \langle \{q_a, d_a^\dagger\}(\tau_1) \rangle \\ &+ \langle T_\tau q_a(\tau_1) [H_{\text{AIM}}, d_a^\dagger](\tau_2) \rangle. \end{aligned} \quad (\text{A21})$$

The anti-commutator $\{q_a, d_a^\dagger\}$ for diagonal hybridization functions follows as:

$$\langle \{q_a, d_a^\dagger\} \rangle = \left\langle \sum_{jkl} U_{[aj]kl} (d_j^\dagger d_l \delta_{ak} - d_j^\dagger \delta_{al} d_k) \right\rangle(\tau_1) \quad (\text{A22})$$

$$= 2 \sum_j U_{[aj][aj]} n_j \quad (\text{A23})$$

The commutator between the local Hamiltonian and the creation operator is calculated in analogy to Eq.(A5)

and follows as:

$$[H_{\text{AIM}}, d_a^\dagger] = q_a^\dagger + \tilde{\varepsilon}_a d_a^\dagger + \sum_K V_K^{aa} c_{Ka}^\dagger. \quad (\text{A24})$$

Thus:

$$\begin{aligned} \partial_{\tau_2} \langle T_\tau q_a(\tau_1) d_a^\dagger(\tau_2) \rangle &= \quad (\text{A25}) \\ &- 2\delta(\tau_1 - \tau_2) \sum_j U_{[aj][aj]} n_j + \langle T_\tau q_a(\tau_1) q_a^\dagger(\tau_2) \rangle \\ &+ \langle T_\tau q_a(\tau_1) \tilde{\varepsilon}_a d_a^\dagger(\tau_2) \rangle + \langle T_\tau q_a(\tau_1) \sum_K V_K^{aa} c_{Ka}^\dagger(\tau_2) \rangle. \end{aligned}$$

The mixed bath-impurity expectation value is calculated in analogy to Eqs.(A14)-(A16) and follows as:

$$\partial_{\tau_2} \langle T_\tau q_a(\tau_1) c_{Ka}^\dagger(\tau_2) \rangle = \langle T_\tau q_a(\tau_1) [H_{\text{AIM}}, c_{Ka}^\dagger](\tau_2) \rangle \quad (\text{A26})$$

$$(\partial_{\tau_2} - \varepsilon_{Ka}) \langle T_\tau q_a(\tau_1) c_{Ka}^\dagger(\tau_2) \rangle = (V_K^{aa})^* \langle T_\tau q_a(\tau_1) d_a^\dagger(\tau_2) \rangle. \quad (\text{A27})$$

This allows one to express the mixed bath-impurity expectation value as an impurity expectation value. Again the equation can be made algebraic by Fourier transforming it, but this time with respect to τ_2 :

$$\begin{aligned} & \int_0^\beta d\tau_2 e^{-i\nu_2 \tau_2} \langle T_\tau q_a(\tau_1) c_{Ka}^\dagger(\tau_2) \rangle \\ &= \frac{(V_K^{aa})^*}{i\nu_2 - \varepsilon_{Ka}} \int_0^\beta d\tau_2 e^{-i\nu_2 \tau_2} \langle T_\tau q_a(\tau_1) d_a^\dagger(\tau_2) \rangle \end{aligned} \quad (\text{A28})$$

Re-inserting into the (Fourier-transformed) Eq.(A25) gives:

$$\begin{aligned} & i\nu_2 \int_0^\beta d\tau_2 e^{-i\nu_2 \tau_2} \langle T_\tau q_a(\tau_1) d_a^\dagger(\tau_2) \rangle \\ &= - \int_0^\beta d\tau_2 e^{-i\nu_2 \tau_2} \delta(\tau_1 - \tau_2) \sum_j U_{[aj][aj]} n_j \\ &+ \int_0^\beta d\tau_2 e^{-i\nu_2 \tau_2} \langle T_\tau q_a(\tau_1) q_a^\dagger(\tau_2) \rangle \\ &+ \tilde{\varepsilon}_a \int_0^\beta d\tau_2 e^{-i\nu_2 \tau_2} \langle T_\tau q_a(\tau_1) d_a^\dagger(\tau_2) \rangle \\ &+ \underbrace{\sum_K \frac{V_K^{aa} (V_K^{aa})^*}{i\nu_2 - \varepsilon_{Ka}}}_{\Delta_a^{\nu_2}} \int_0^\beta d\tau_2 e^{-i\nu_2 \tau_2} \langle T_\tau q_a(\tau_1) d_a^\dagger(\tau_2) \rangle \end{aligned}$$

Rearranging gives:

$$\begin{aligned} & \underbrace{(i\nu_2 - \tilde{\varepsilon}_a - \Delta_a^{\nu_2})}_{[\mathcal{G}_a^{\nu_2}]^{-1}} \int_0^\beta d\tau_2 e^{-i\nu_2 \tau_2} \langle T_\tau q_a(\tau_1) d_a^\dagger(\tau_2) \rangle \\ &= - \int_0^\beta d\tau_2 e^{-i\nu_2 \tau_2} [2 \sum_j U_{[aj][aj]} n_j \delta(\tau_1 - \tau_2) \\ &- \langle T_\tau q_a(\tau_1) q_a^\dagger(\tau_2) \rangle] \end{aligned} \quad (\text{A29})$$

Together with the definitions of Table I we obtain the one-particle symmetric improved estimator Eq. (13):

$$G_a^\nu = \mathcal{G}_a^\nu + [\mathcal{G}_a^\nu]^2 (2 \sum_j U_{[aj][aj]} n_j + \vartheta_a^\nu). \quad (\text{A30})$$

Appendix B: Two-particle Symmetric Improved Estimator

In the following we derive the two-particle symmetric improved estimators. Again the conventional improved estimators were already derived in Ref. 16. The procedure in deriving the higher order (up to fourth-order) equations is in principle equivalent to the one-particle symmetric improved estimators. Nevertheless, the equations are more involved due to the necessity of considering multiple hierarchies of equations of motions. Repeating derivations (such as the explicit calculation of mixed impurity-bath expectation values) are omitted.

First Order

Applying the time derivative onto the first annihilation operator of the two-particle Green's function gives:

$$\begin{aligned} \partial_{\tau_1} G_{abcd}^{\tau_1, \tau_2, \tau_3, \tau_4} = \\ R_1 + \langle T_\tau \underbrace{[H_{\text{AIM}}, d_a]}_{-q_a - \tilde{\varepsilon}_a d_a - \sum_K (V_K^{aa})^* c_{K a}}(\tau_1) d_b^\dagger(\tau_2) d_c(\tau_3) d_d^\dagger(\tau_4) \rangle \quad (\text{B1}) \end{aligned}$$

$$\begin{aligned} (\partial_{\tau_1} + \tilde{\varepsilon}_a) G_{abcd}^{\tau_1, \tau_2, \tau_3, \tau_4} = \\ R_1 - \underbrace{\langle T_\tau q_a(\tau_1) d_b^\dagger(\tau_2) d_c(\tau_3) d_d^\dagger(\tau_4) \rangle}_{=: S_1} \\ - \underbrace{\langle T_\tau \sum_K (V_K^{aa})^* c_{K a}(\tau_1) d_b^\dagger(\tau_2) d_c(\tau_3) d_d^\dagger(\tau_4) \rangle}_{\rightarrow \Delta_a^{\nu_1} G_{abcd}^{\nu_1, \tau_2, \tau_3, \tau_4}} \quad (\text{B2}) \end{aligned}$$

Again, Fourier transformation with respect to the first time argument converts the differential equation to an algebraic one, and we have

$$G_{abcd}^{\nu_1, \tau_2, \tau_3, \tau_4} = \mathcal{G}_a^{\nu_1} \left(-R_{1,abcd}^{\nu_1, \tau_2, \tau_3, \tau_4} + S_{1,abcd}^{\nu_1, \tau_2, \tau_3, \tau_4} \right). \quad (\text{B3})$$

R_1 describes the equal-time contribution due to the derivation of the time-ordering operator:

$$\begin{aligned} R_{1,abcd}^{\tau_1, \tau_2, \tau_3, \tau_4} = \delta(\tau_1 - \tau_2) \langle T_\tau \{d_a, d_b^\dagger\}(\tau_1) d_c(\tau_3) d_d^\dagger(\tau_4) \rangle + \\ \delta(\tau_1 - \tau_4) \langle T_\tau \{d_a, d_d^\dagger\}(\tau_1) d_b^\dagger(\tau_2) d_c(\tau_3) \rangle \quad (\text{B4}) \end{aligned}$$

$$\begin{aligned} = \delta(\tau_1 - \tau_2) \delta_{ab} \underbrace{\langle T_\tau d_c(\tau_3) d_d^\dagger(\tau_4) \rangle}_{-G_{cd}^{\tau_3 \tau_4}} \\ - \delta(\tau_1 - \tau_4) \delta_{ad} \underbrace{\langle T_\tau d_c(\tau_3) d_b^\dagger(\tau_2) \rangle}_{-G_{cb}^{\tau_3 \tau_2}} \quad (\text{B5}) \end{aligned}$$

At this stage one can already observe that it is possible to apply further (imaginary) time derivatives, or equivalently, hierarchies of equations of motion onto the R_1 term. The corresponding time-derivatives of the one-particle Green's function are given by the one-particle symmetric improved estimators and were already calculated explicitly in Appendix A.

Second Order

Applying the time derivative onto the first creation operator of S_1 gives:

$$\begin{aligned} \partial_{\tau_2} S_1 = \\ R_2 + \langle T_\tau q_a(\tau_1) \underbrace{[H_{\text{AIM}}, d_b^\dagger]}_{q_b^\dagger + \tilde{\varepsilon}_b d_b^\dagger + \sum_K V_K^{bb} c_{K b}^\dagger}(\tau_2) d_c(\tau_3) d_d^\dagger(\tau_4) \rangle \quad (\text{B6}) \end{aligned}$$

$$\begin{aligned} (\partial_{\tau_2} - \tilde{\varepsilon}_b) S_1 = \\ R_2 + \underbrace{\langle T_\tau q_a(\tau_1) q_b^\dagger(\tau_2) d_c(\tau_3) d_d^\dagger(\tau_4) \rangle}_{=: S_2} \\ + \underbrace{\langle T_\tau q_a(\tau_1) \sum_K V_K^{bb} c_{K b}^\dagger(\tau_2) d_c(\tau_3) d_d^\dagger(\tau_4) \rangle}_{\rightarrow \Delta_b^{\nu_2} S_1^{\tau_1, \nu_2, \tau_3, \tau_4}} \quad (\text{B7}) \end{aligned}$$

$$S_1^{\tau_1, \nu_2, \tau_3, \tau_4} = \mathcal{G}_b^{\nu_2} (R_2^{\tau_1, \nu_2, \tau_3, \tau_4} + S_2^{\tau_1, \nu_2, \tau_3, \tau_4}) \quad (\text{B8})$$

Fourier-transforming this also with respect to τ_1 and plugging it into Eq. (B3) yields:

$$\begin{aligned} G_{abcd}^{\nu_1, \nu_2, \tau_3, \tau_4} = \mathcal{G}_a^{\nu_1} \left(-R_{1,abcd}^{\nu_1, \nu_2, \tau_3, \tau_4} + \mathcal{G}_b^{\nu_2} \times \right. \\ \left. \left(R_{2,abcd}^{\nu_1, \nu_2, \tau_3, \tau_4} + S_{2,abcd}^{\nu_1, \nu_2, \tau_3, \tau_4} \right) \right) \quad (\text{B9}) \end{aligned}$$

R_2 describes the equal-time contribution due to the derivation of the time-ordering operator of S_1 :

$$\begin{aligned} R_{2,abcd}^{\tau_1, \tau_2, \tau_3, \tau_4} = -\delta(\tau_1 - \tau_2) \langle T_\tau \{q_a, d_b^\dagger\}(\tau_1) d_c(\tau_3) d_d^\dagger(\tau_4) \rangle \\ + 2 \sum_{ef} U_{[ae][bf]} d_e^\dagger d_f \\ + \delta(\tau_2 - \tau_3) \langle T_\tau q_a(\tau_1) \{d_b^\dagger, d_c\}(\tau_2) d_d^\dagger(\tau_4) \rangle \quad (\text{B10}) \end{aligned}$$

$$\begin{aligned} = -2\delta(\tau_1 - \tau_2) \langle T_\tau \sum_{ef} U_{[ae][bf]} d_e^\dagger d_f(\tau_1) d_c(\tau_3) d_d^\dagger(\tau_4) \rangle \\ + \delta(\tau_2 - \tau_3) \delta_{bc} \langle T_\tau q_a(\tau_1) d_d^\dagger(\tau_4) \rangle \quad (\text{B11}) \end{aligned}$$

Time derivatives of R_2 with respect to τ_3 and τ_4 are shown below.

Third Order

Applying the time derivative onto the remaining annihilation operator of S_2 gives:

$$\begin{aligned} \partial_{\tau_3} S_2 = & R_3 + \langle T_{\tau} q_a(\tau_1) q_b^{\dagger}(\tau_2) \underbrace{[H_{\text{AIM}}, d_c]}_{-q_c - \tilde{\varepsilon}_c d_c - \sum_K (V_K^{cc})^* c_{Kc}}(\tau_3) d_d^{\dagger}(\tau_4) \rangle \\ & \text{(B12)} \end{aligned}$$

$$\begin{aligned} (\partial_{\tau_3} + \tilde{\varepsilon}_c) S_2 = & R_3 - \underbrace{\langle T_{\tau} q_a(\tau_1) q_b^{\dagger}(\tau_2) q_c(\tau_3) d_d^{\dagger}(\tau_4) \rangle}_{=: S_3} \\ & - \underbrace{\langle T_{\tau} q_a(\tau_1) q_b^{\dagger}(\tau_2) \sum_K (V_K^{cc})^* c_{Kc}(\tau_3) d_d^{\dagger}(\tau_4) \rangle}_{\rightarrow \Delta_c^{\nu_3} S_2} \\ & \text{(B13)} \end{aligned}$$

$$S_{2,abcd}^{\tau_1, \tau_2, \nu_3, \tau_4} = \mathcal{G}_c^{\nu_3} \left(-R_{3,abcd}^{\tau_1, \tau_2, \nu_3, \tau_4} + S_{3,abcd}^{\tau_1, \tau_2, \nu_3, \tau_4} \right) \quad \text{(B14)}$$

Fourier-transforming this expression for S_2 now also with respect to τ_1 and τ_2 , and plugging it into Eq. (B9) yields:

$$\begin{aligned} G_{abcd}^{\nu_1, \nu_2, \nu_3, \tau_4} = & \mathcal{G}_a^{\nu_1} \left(-R_{1,abcd}^{\nu_1, \nu_2, \nu_3, \tau_4} + \mathcal{G}_b^{\nu_2} \times \right. \\ & \left. (R_{2,abcd}^{\nu_1, \nu_2, \nu_3, \tau_4} + \mathcal{G}_c^{\nu_3} (-R_{3,abcd}^{\nu_1, \nu_2, \nu_3, \tau_4} + S_{3,abcd}^{\nu_1, \nu_2, \nu_3, \tau_4})) \right) \\ & \text{(B15)} \end{aligned}$$

R_3 describes the equal-time contribution due to the derivation of the time-ordering operator of S_2 :

$$\begin{aligned} R_{3,abcd}^{\tau_1, \tau_2, \tau_3, \tau_4} = & \delta(\tau_1 - \tau_3) \langle T_{\tau} \underbrace{\{q_a, d_c\}}_{\sum_{fg} U_{[ac]fg} d_g d_f}(\tau_1) q_b^{\dagger}(\tau_2) d_d^{\dagger}(\tau_4) \rangle \\ & - \delta(\tau_2 - \tau_3) \langle T_{\tau} q_a(\tau_1) \underbrace{\{q_b^{\dagger}, d_c\}}_{2 \sum_{ij} U_{[ci][bj]} d_i^{\dagger} d_j}(\tau_2) d_d^{\dagger}(\tau_4) \rangle \\ & + \delta(\tau_3 - \tau_4) \langle T_{\tau} q_a(\tau_1) q_b^{\dagger}(\tau_2) \{d_c, d_d^{\dagger}\}(\tau_3) \rangle \quad \text{(B16)} \\ = & \delta(\tau_1 - \tau_3) \langle T_{\tau} \sum_{fg} U_{[ac]fg} d_g d_f(\tau_1) q_b^{\dagger}(\tau_2) d_d^{\dagger}(\tau_4) \rangle \\ & - 2\delta(\tau_2 - \tau_3) \langle T_{\tau} q_a(\tau_1) \sum_{ij} U_{[ci][bj]} d_i^{\dagger} d_j(\tau_2) d_d^{\dagger}(\tau_4) \rangle \\ & + \delta(\tau_3 - \tau_4) \delta_{cd} \langle T_{\tau} q_a(\tau_1) q_b^{\dagger}(\tau_2) \rangle \quad \text{(B17)} \end{aligned}$$

Time derivatives of R_3 with respect to τ_4 are shown below.

Fourth Order

Applying the time derivative onto the remaining creation operator of S_3 gives:

$$\begin{aligned} \partial_{\tau_4} S_3 = & R_4 + \langle T_{\tau} q_a(\tau_1) q_b^{\dagger}(\tau_2) q_c(\tau_3) \underbrace{[H_{\text{AIM}}, d_d^{\dagger}]}_{q_d^{\dagger} + \tilde{\varepsilon}_d d_d^{\dagger} + \sum_K V_K^{dd} c_{Kd}^{\dagger}}(\tau_4) \rangle \\ & \text{(B18)} \end{aligned}$$

$$\begin{aligned} (\partial_{\tau_4} - \tilde{\varepsilon}_d) S_3 = & R_4 + \underbrace{\langle T_{\tau} q_a(\tau_1) q_b^{\dagger}(\tau_2) q_c(\tau_3) q_d^{\dagger}(\tau_4) \rangle}_{=: S_4} \\ & + \underbrace{\langle T_{\tau} q_a(\tau_1) q_b^{\dagger}(\tau_2) q_c(\tau_3) \sum_K V_K^{dd} c_{Kd}^{\dagger}(\tau_4) \rangle}_{\rightarrow \Delta_d^{\nu_4} S_3} \\ & \text{(B19)} \end{aligned}$$

$$S_{3,abcd}^{\tau_1, \tau_2, \tau_3, \nu_4} = \mathcal{G}_d^{\nu_4} \left(R_{4,abcd}^{\tau_1, \tau_2, \tau_3, \nu_4} + S_{4,abcd}^{\tau_1, \tau_2, \tau_3, \nu_4} \right) \quad \text{(B20)}$$

Fourier-transforming S_3 with respect to the remaining time arguments and inserting it into Eq. (B15) yields:

$$\begin{aligned} G_{abcd}^{\nu_1, \nu_2, \nu_3, \nu_4} = & \mathcal{G}_a^{\nu_1} \left[-R_{1,abcd}^{\nu_1, \nu_2, \nu_3, \nu_4} + \mathcal{G}_b^{\nu_2} \times \right. \\ & \left. [R_{2,abcd}^{\nu_1, \nu_2, \nu_3, \nu_4} + \mathcal{G}_c^{\nu_3} (-R_{3,abcd}^{\nu_1, \nu_2, \nu_3, \nu_4} + \mathcal{G}_d^{\nu_4} \times \right. \\ & \left. (R_{4,abcd}^{\nu_1, \nu_2, \nu_3, \nu_4} + S_{4,abcd}^{\nu_1, \nu_2, \nu_3, \nu_4})) \right], \quad \text{(B21)} \end{aligned}$$

where $S_{4,abcd}^{\nu_1, \nu_2, \nu_3, \nu_4} = h_{abcd}^{\nu_1, \nu_2, \nu_3, \nu_4} / \beta$, as defined in Table I. R_4 describes the equal-time contribution due to the derivation of the time-ordering operator of S_3 :

$$\begin{aligned} R_{4,abcd}^{\tau_1, \tau_2, \tau_3, \tau_4} = & -\delta(\tau_1 - \tau_4) \langle T_{\tau} \underbrace{\{q_a, d_d^{\dagger}\}}_{2 \sum_{ef} U_{[ae][df]} d_e^{\dagger} d_f}(\tau_1) q_b^{\dagger}(\tau_2) q_c(\tau_3) \rangle \\ & + \delta(\tau_2 - \tau_4) \langle T_{\tau} q_a(\tau_1) \underbrace{\{q_b^{\dagger}, d_d^{\dagger}\}}_{\sum_{hi} U_{hi[bd]} d_h^{\dagger} d_i^{\dagger}}(\tau_2) q_c(\tau_3) \rangle \\ & - \delta(\tau_3 - \tau_4) \langle T_{\tau} q_a(\tau_1) q_b^{\dagger}(\tau_2) \underbrace{\{q_c, d_d^{\dagger}\}}_{2 \sum_{kl} U_{[ck][dl]} d_k^{\dagger} d_l}(\tau_3) \rangle \quad \text{(B22)} \\ = & -2\delta(\tau_1 - \tau_4) \langle T_{\tau} \sum_{ef} U_{[ae][df]} d_e^{\dagger} d_f(\tau_1) q_b^{\dagger}(\tau_2) q_c(\tau_3) \rangle \\ & + \delta(\tau_2 - \tau_4) \langle T_{\tau} q_a(\tau_1) \sum_{hi} U_{hi[bd]} d_h^{\dagger} d_i^{\dagger}(\tau_2) q_c(\tau_3) \rangle \\ & - 2\delta(\tau_3 - \tau_4) \langle T_{\tau} q_a(\tau_1) q_b^{\dagger}(\tau_2) \sum_{kl} U_{[ck][dl]} d_k^{\dagger} d_l(\tau_3) \rangle \\ & \text{(B23)} \end{aligned}$$

Unlike the previous terms R_1, R_2, R_3 , the above R_4 cannot be derived any further.

Third and fourth order of R_2 and R_3

Looking at equation Eq. (B21) one notices that in fact only R_4 and S_4 are multiplied by a product of four non-interacting Green's functions. R_1 consists of one-particle Green's functions, which can be expressed by their symmetric improved estimators. However, R_2 and R_3 are multiplied only by products of 2 and 3 non-interacting Green's functions, respectively. This means that we need to express them by their equations of motion recursively. First, let us take a closer look at the first term of R_2 , Eq. (B11). It is very similar to the three-leg Green's function of Eq. (27), the only difference being in the operator ordering and the additional U -matrix. The following steps may therefore also serve as a derivation of the threeleg improved estimator. Taking the time-derivative with respect to τ_3 generically yields

$$\begin{aligned} & \partial_{\tau_3} \langle T_{\tau} \sum_{ef} U_{[ae][bf]} d_e^{\dagger} d_f(\tau_1) d_c(\tau_3) d_d^{\dagger}(\tau_4) \rangle \\ &= R_{21} + \langle T_{\tau} \sum_{ef} U_{[ae][bf]} d_e^{\dagger} d_f(\tau_1) \partial_{\tau_3} d_c(\tau_3) d_d^{\dagger}(\tau_4) \rangle \quad (\text{B24}) \end{aligned}$$

Analogously as before, we express the time derivative by the Heisenberg equation of motion and Fourier-transform the equation with respect to τ_3 to make it algebraic. We thus obtain

$$\begin{aligned} & \int_0^{\beta} d\tau_3 e^{i\nu_3\tau_3} \langle \sum_{ef} U_{[ae][bf]} d_e^{\dagger} d_f(\tau_1) d_c(\tau_3) d_d^{\dagger}(\tau_4) \rangle \\ &= \mathcal{G}_c^{\nu_3} \int_0^{\beta} d\tau_3 e^{i\nu_3\tau_3} [-R_{21}^{\tau_1, \tau_3, \tau_4} \\ & \quad + \langle \sum_{ef} U_{[ae][bf]} d_e^{\dagger} d_f(\tau_1) q_c(\tau_3) d_d^{\dagger}(\tau_4) \rangle] \quad (\text{B25}) \end{aligned}$$

The rest-term R_{21} that originates from the derivative of the time-ordering operator, is

$$\begin{aligned} R_{21}^{\tau_1, \tau_3, \tau_4} &= \delta(\tau_1 - \tau_3) \langle T_{\tau} [\sum_{ef} U_{[ae][bf]} d_e^{\dagger} d_f, d_c](\tau_3) d_d^{\dagger}(\tau_4) \rangle \\ & \quad + \delta(\tau_3 - \tau_4) \langle T_{\tau} \sum_{ef} U_{[ae][bf]} d_e^{\dagger} d_f \{ d_c, d_d^{\dagger} \}(\tau_3) \rangle. \quad (\text{B26}) \end{aligned}$$

We want to emphasize that due to the bosonic operator $d^{\dagger}d$, a commutator occurs in the first line. After evaluation of the commutator and anti-commutator, we get

$$\begin{aligned} R_{21}^{\tau_1, \tau_3, \tau_4} &= \delta(\tau_1 - \tau_3) U_{[ac][bd]} \langle T_{\tau} d_d(\tau_1) d_d^{\dagger}(\tau_4) \rangle \\ & \quad + \delta(\tau_3 - \tau_4) \delta_{cd} \sum_{ef} U_{[ae][bf]} n_{ef} \quad (\text{B27}) \end{aligned}$$

In order to obtain the final form, we also have to apply the equation of motion with respect to τ_4 . In R_{21} this

concerns only the first term. This is, however, just a one-particle Green's function and we can insert the improved-estimator formula Eq. (9) and we thus get

$$\begin{aligned} R_{21}^{\tau_1, \tau_3, \nu_4} &= \delta(\tau_1 - \tau_3) \sum_f U_{[ac][bf]} \mathcal{G}_d^{\nu_4} [-e^{-i\nu_4\tau_1} \delta_{fd} \\ & \quad + \int_0^{\beta} d\tau_4 e^{-i\nu_4\tau_4} \langle T_{\tau} d_f(\tau_1) q_d^{\dagger}(\tau_4) \rangle] \\ & \quad + e^{-i\nu_4\tau_3} \delta_{cd} \sum_{ef} U_{[ae][bf]} n_{ef} \quad (\text{B28}) \end{aligned}$$

Whereas the rest-term R_{21} contains only the one-particle improved estimator and the occupation number, we can differentiate the last term in equation Eq. (B25) by its last time argument τ_4 . The same procedure as above yields now

$$\begin{aligned} & \int_0^{\beta} d\tau_4 e^{-i\nu_4\tau_4} \langle \sum_{ef} U_{[ae][bf]} d_e^{\dagger} d_f(\tau_1) q_c(\tau_3) d_d^{\dagger}(\tau_4) \rangle \\ &= \mathcal{G}_d^{\nu_4} \int_0^{\beta} d\tau_4 e^{-i\nu_4\tau_4} [R_{22}^{\tau_1, \tau_3, \tau_4} \\ & \quad + \langle \sum_{ef} U_{[ae][bf]} d_e^{\dagger} d_f(\tau_1) q_c(\tau_3) q_d^{\dagger}(\tau_4) \rangle] \quad (\text{B29}) \end{aligned}$$

The rest-term R_{22} again requires some precaution, since it contains both a commutator and an anti-commutator:

$$\begin{aligned} R_{22}^{\tau_1, \tau_3, \tau_4} &= \delta(\tau_1 - \tau_4) \langle T_{\tau} [\sum_{ef} U_{[ae][bf]} d_e^{\dagger} d_f, d_d^{\dagger}](\tau_1) q_c(\tau_3) \rangle \\ & \quad - \delta(\tau_3 - \tau_4) \langle T_{\tau} \sum_{ef} U_{[ae][bf]} d_e^{\dagger} d_f(\tau_1) \{ q_c, d_d^{\dagger} \}(\tau_3) \rangle \quad (\text{B30}) \end{aligned}$$

After evaluation of the commutator and the anti-commutator, we obtain

$$\begin{aligned} R_{22}^{\tau_1, \tau_3, \tau_4} &= \delta(\tau_1 - \tau_4) \langle T_{\tau} \sum_e U_{[ae][bd]} d_e^{\dagger}(\tau_1) q_c(\tau_3) \rangle \\ & \quad - 2\delta(\tau_3 - \tau_4) \langle \sum_{ef} U_{[ae][bf]} d_e^{\dagger} d_f(\tau_1) \sum_{gh} U_{[ag][bh]} d_g^{\dagger} d_h(\tau_3) \rangle. \quad (\text{B31}) \end{aligned}$$

We are now able to write down the full expression for R_2 by combining Eq. (B11) with Eq. (B28) and Eq. (B31). Since in the end we need it in Matsubara frequencies, it is of advantage to perform a Fourier transform with respect to all time arguments already here. Furthermore this allows us to make the equation more compact by using the definitions of Table I and the relation $\langle T_{\tau} q_j(\tau) d_k^{\dagger} \rangle = \langle T_{\tau} d_k(\tau) q_j^{\dagger} \rangle$, such that we finally arrive at Eq. (21).

For R_3 we only have to apply the equation of motion with respect to τ_4 to the first two terms of Eq. (B17). Again we perform a Fourier transform with respect to all time arguments and compactify the expression by the definitions of Table I. Thus, we obtain Eq. (22).

Appendix C: Lehmann representations for two-frequency objects

For objects depending on a single fermionic/bosonic frequency, the standard Lehmann representations for fermionic/bosonic Green's functions can be used. For objects depending on two fermionic and one bosonic Green's function, we use the form published in [29]. Additionally, we need it for

$$f^{\nu\omega} = \int_0^\beta d\tau_1 d\tau_2 d\tau_3 e^{i[\nu(\tau_1-\tau_2)+\omega(\tau_2-\tau_3)]} \times \langle \mathcal{T}_\tau F_1(\tau_1) F_2(\tau_2) B(\tau_3) \rangle \quad (\text{C1})$$

Here, F_i (B) are fermionic (bosonic) operators, and ν (ω) are fermionic (bosonic) frequencies. Inserting the eigenbasis of the Hamiltonian and evaluating the integrals analytically, we obtain

$$\begin{aligned} f^{\nu\omega} &= \frac{1}{Z} \sum_{mnl} F_1^{mn} F_2^{nl} B^{lm} \frac{1}{-i\nu + i\omega + E_n - E_l} \\ &\times \left[\frac{e^{-\beta E_l} - e^{-\beta E_m}}{i\omega + E_m - E_l} + \frac{e^{-\beta E_n} + e^{-\beta E_m}}{i\nu + E_m - E_n} \right] \\ &+ \frac{1}{Z} \sum_{mnl} F_2^{mn} F_1^{nl} B^{lm} \frac{1}{i\nu + E_n - E_l} \\ &\times \left[\frac{e^{-\beta E_l} - e^{-\beta E_m}}{i\omega + E_m - E_l} + \frac{e^{-\beta E_n} + e^{-\beta E_m}}{-i\nu + i\omega + E_m - E_n} \right] \end{aligned} \quad (\text{C2})$$

Furthermore, we need

$$g^{\nu\omega} = \int_0^\beta d\tau_1 d\tau_2 d\tau_3 e^{i[\nu_1(\tau_1-\tau_3)+\nu_2(\tau_2-\tau_3)]} \times \langle \mathcal{T}_\tau F_1(\tau_1) F_2(\tau_2) B(\tau_3) \rangle. \quad (\text{C3})$$

with two fermionic frequencies ν_1, ν_2 . The result is

$$\begin{aligned} g^{\nu\omega} &= \frac{1}{Z} \sum_{mkl} F_1^{mn} F_2^{nl} B^{lm} \frac{1}{i\nu_2 + E_n - E_l} \\ &\times \left[\frac{e^{-\beta E_l} - e^{-\beta E_m}}{i\nu_1 + i\nu_2 + E_m - E_l} + \frac{e^{-\beta E_n} + e^{-\beta E_m}}{i\nu_1 + E_m - E_n} \right] \\ &+ \frac{1}{Z} \sum_{mnl} F_2^{mn} F_1^{nl} B^{lm} \frac{1}{i\nu_1 + E_n - E_l} \\ &\times \left[\frac{e^{-\beta E_l} - e^{-\beta E_m}}{i\nu_1 + i\nu_2 + E_m - E_l} + \frac{e^{-\beta E_n} + e^{-\beta E_m}}{i\nu_2 + E_m - E_n} \right] \end{aligned} \quad (\text{C4})$$

-
- [1] J. Hubbard, Electron correlations in narrow energy bands. III. An improved solution, Proc R. Soc. London **281**, 401 (1964).
- [2] P. W. Anderson, Localized Magnetic States in Metals, Physical Review **124**, 41 (1961).
- [3] A. Georges, G. Kotliar, W. Krauth, and M. J. Rozenberg, Dynamical mean-field theory of strongly correlated fermion systems and the limit of infinite dimensions, Rev. Mod. Phys. **68**, 13 (1996).
- [4] E. Gull, A. J. Millis, A. I. Lichtenstein, A. N. Rubtsov, M. Troyer, and P. Werner, Continuous-time monte carlo methods for quantum impurity models, Reviews of Modern Physics **83**, 349 (2011).
- [5] E. Gull, *Continuous-time quantum Monte Carlo algorithms for fermions*, Ph.D. thesis, ETH Zurich (2008).
- [6] P. Gunacker, M. Wallerberger, E. Gull, A. Hausoel, G. Sangiovanni, and K. Held, Continuous-time quantum monte carlo using worm sampling, Phys. Rev. B **92**, 155102 (2015).
- [7] A. Rubtsov and A. Lichtenstein, Continuous-time quantum monte carlo method for fermions: Beyond auxiliary field framework, Journal of Experimental and Theoretical Physics Letters **80**, 61 (2004).
- [8] E. Gull, P. Werner, O. Parcollet, and M. Troyer, Continuous-time auxiliary-field monte carlo for quantum impurity models, EPL (Europhysics Letters) **82**, 57003 (2008).
- [9] P. Werner, A. Comanac, L. de' Medici, M. Troyer, and A. J. Millis, Continuous-time solver for quantum impurity models, Phys. Rev. Lett. **97**, 076405 (2006).
- [10] E. Gull, P. Werner, A. Millis, and M. Troyer, Performance analysis of continuous-time solvers for quantum impurity models, Phys. Rev. B **76**, 235123 (2007).
- [11] L. Boehnke, H. Hafermann, M. Ferrero, F. Lechermann, and O. Parcollet, Orthogonal polynomial representation of imaginary-time green's functions, Phys. Rev. B **84**, 075145 (2011).
- [12] M. Potthoff, T. Wegner, and W. Nolting, Interpolating self-energy of the infinite-dimensional hubbard model: Modifying the iterative perturbation theory, Phys. Rev. B **55**, 16132 (1997).
- [13] X. Wang, H. T. Dang, and A. J. Millis, High-frequency asymptotic behavior of self-energies in quantum impurity models, Phys. Rev. B **84**, 073104 (2011).
- [14] N. Wentzell, G. Li, A. Tagliavini, C. Taranto, G. Rohringer, K. Held, A. Toschi, and S. Andergassen, High-frequency asymptotics of the vertex function: diagrammatic parametrization and algorithmic implementation, arXiv (2016), 1610.06520.
- [15] J. Kaufmann, P. Gunacker, and K. Held, Continuous-time quantum monte carlo calculation of multiorbital vertex asymptotics, Phys. Rev. B **96**, 035114 (2017).
- [16] H. Hafermann, K. R. Patton, and P. Werner, Improved estimators for the self-energy and vertex function in hybridization-expansion continuous-time quan-

- tum monte carlo simulations, *Phys. Rev. B* **85**, 205106 (2012).
- [17] H. Hafermann, Self-energy and vertex functions from hybridization-expansion continuous-time quantum monte carlo for impurity models with retarded interaction, *Phys. Rev. B* **89**, 235128 (2014).
- [18] P. Gunacker, M. Wallerberger, T. Ribic, A. Hausoel, G. Sangiovanni, and K. Held, Worm-improved estimators in continuous-time quantum monte carlo, *Phys. Rev. B* **94**, 125153 (2016).
- [19] G. Górski and J. Mizia, Equation of motion solutions to hubbard model retaining kondo effect, *Physica B: Condensed Matter* **427**, 42 (2013).
- [20] A. Moutenet, W. Wu, and M. Ferrero, Determinant monte carlo algorithms for dynamical quantities in fermionic systems, *Phys. Rev. B* **97**, 085117 (2018).
- [21] P. Werner and A. J. Millis, Hybridization expansion impurity solver: General formulation and application to kondo lattice and two-orbital models, *Phys. Rev. B* **74**, 155107 (2006).
- [22] T. Matsubara, A new approach to quantum-statistical mechanics, *Prog. Theor. Phys.* **14**, 351 (1955).
- [23] R. Bulla, A. C. Hewson, and T. Pruschke, Numerical renormalization group calculations for the self energy of the impurity anderson model, *J. Phys.: Condens. Matter* **10**, 8365 (1998).
- [24] One may also refer to ξ as $G\Sigma$.
- [25] M. Wallerberger, *PhD Thesis* (TU Wien, 2016).
- [26] G. Rohringer, H. Hafermann, A. Toschi, A. A. Katanin, A. E. Antipov, M. I. Katsnelson, A. I. Lichtenstein, A. N. Rubtsov, and K. Held, Diagrammatic routes to non-local correlations beyond dynamical mean field theory, *Rev. Mod. Phys.* **90**, 025003 (2018), arXiv:1705.00024 [cond-mat.str-el].
- [27] A. Georges, G. Kotliar, W. Krauth, and M. J. Rozenberg, Dynamical mean-field theory of strongly correlated fermion systems and the limit of infinite dimensions, *Rev. Mod. Phys.* **68**, 13.
- [28] J. Kuneš, Efficient treatment of two-particle vertices in dynamical mean-field theory, *Phys. Rev. B* **83**, 085102 (2011).
- [29] A. Toschi, A. A. Katanin, and K. Held, Dynamical vertex approximation: A step beyond dynamical mean-field theory, *Phys. Rev. B* **75**, 045118 (2007).
- [30] A. N. Rubtsov, M. I. Katsnelson, and A. I. Lichtenstein, Dual fermion approach to nonlocal correlations in the hubbard model, *Phys. Rev. B* **77**, 033101 (2008).
- [31] A. A. Katanin, A. Toschi, and K. Held, Comparing pertinent effects of antiferromagnetic fluctuations in the two- and three-dimensional hubbard model, *Phys. Rev. B* **80**, 075104 (2009).
- [32] A. N. Rubtsov, M. I. Katsnelson, and A. I. Lichtenstein, Dual boson approach to collective excitations in correlated fermionic systems, *Ann. Phys.* **327**, 1320 (2012).
- [33] T. Ayrál and O. Parcollet, Mott physics and spin fluctuations: A unified framework, *Phys. Rev. B* **92**, 115109 (2015).
- [34] A. Galler, P. Thunström, P. Gunacker, J. M. Tomczak, and K. Held, Ab initio dynamical vertex approximation, arXiv:1610.02998 (2016).
- [35] E. G. C. P. van Loon, F. Krien, H. Hafermann, A. I. Lichtenstein, and M. I. Katsnelson, Fermion-boson vertex within dynamical mean-field theory, *Phys. Rev. B* **98**, 205148 (2018).
- [36] G. Li, N. Wentzell, P. Pudleiner, P. Thunström, and K. Held, Efficient implementation of the parquet equations – role of the reducible vertex function and its kernel approximation, *Phys. Rev. B* **93**, 195134 (2016).
- [37] M. Wallerberger, A. Hausoel, P. Gunacker, A. Kowalski, N. Parragh, F. Goth, K. Held, and G. Sangiovanni, w2dynamics: Local one- and two-particle quantities from dynamical mean field theory, *Computer Physics Communications* **235**, 388 (2019).
- [38] H. Shinaoka, M. Dolfi, M. Troyer, and P. Werner, Hybridization expansion monte carlo simulation of multi-orbital quantum impurity problems: matrix product formalism and improved sampling, *Journal of Statistical Mechanics: Theory and Experiment* **2014**, P06012 (2014).